0026-895X/11/8002-219–227$25.00
MOLECULAR PHARMACOLOGY
Copyright © 2011 The American Society for Pharmacology and Experimental Therapeutics
Mol Pharmacol 80:219–227, 2011

Vol. 80, No. 2
71779/3699850
Printed in U.S.A.

Orientation of μ-Conotoxin PIIIA in a Sodium Channel Vestibule, Based on Voltage Dependence of Its Binding

J. R. McArthur, G. Singh, M. L. O'Mara, D. McMaster, V. Ostroumov, D. P. Tieleman, and R. J. French

Department of Physiology and Pharmacology (J.R.M., D.M., V.O., R.J.F.), the Hotchkiss Brain Institute (J.R.M., D.M., V.O., R.J.F.), and Department of Biological Sciences (G.S., M.L.O., D.P.T.), University of Calgary, Calgary, Canada; and the School of Chemistry and Molecular Biosciences, the University of Queensland, Brisbane, Australia (M.L.O.)

Received February 23, 2011; accepted April 26, 2011

ABSTRACT

Mutant cycle analysis has been used in previous studies to constrain possible docking orientations for various toxins. As an independent test of the bound orientation of μ-conotoxin PIIIA, a selectively targeted sodium channel pore blocker, we determined the contributions to binding voltage dependence of specific residues on the surface of the toxin. A change in the "apparent valence" ($z\delta$) of the block, which is associated with a change of a specific toxin charge, reflects a change in the charge movement within the transmembrane electric field as the toxin binds. Toxin derivatives with charge-conserving mutations (R12K, R14K, and K17R) showed $z\delta$ values similar to those of wild type (0.61 ± 0.01, mean ± S.E.M.). Charge-changing mutations produced a range of responses. Neutralizing substitutions for Arg14 and Lys17 showed the largest reductions in $z\delta$ values, to 0.18 ± 0.06 and 0.20 ± 0.06, respectively, whereas unit charge-changing substitutions for Arg12, Ser13, and Arg20 gave intermediate values (0.24 ± 0.07, 0.33 ± 0.04, and 0.32 ± 0.05), which suggests that each of these residues contributes to the dependence of binding on the transmembrane voltage. Two mutations, R2A and G6K, yielded no significant change in $z\delta$. These observations suggest that the toxin binds with Arg2 and Gly6 facing the extracellular solution, and Arg14 and Lys17 positioned most deeply in the pore. In this study, we used molecular dynamics to simulate toxin docking and performed Poisson-Boltzmann calculations to estimate the changes in local electrostatic potential when individual charges were substituted on the toxin's surface. Consideration of two limiting possibilities suggests that most of the charge movement associated with toxin binding reflects sodium redistribution within the narrow part of the pore.

Introduction

Voltage-gated sodium (Na_v) channels underlie the fast electrical signaling in the nervous system and excitation in heart and skeletal muscle. Na_v channel gain-of-function mutations leading to hyperexcitability causes such maladies as pain, myotonia, epilepsy, and cardiac arrhythmia, and thus Na_v channels are excellent candidates for targeting by inhibitory therapeutic drugs. By targeting different Na_v channel isoforms, it may be possible to provide a technique to control these disorders with minimal side effects. μ-Conotoxins (μCTXs) show striking isoform selectivity among different Na_v channels. μCTXs inhibit current through Na_v channels by binding to toxin site 1 in the outer vestibule of the channel [for an overview of Na_v channel binding sites, see Catterall et al. (2005) and Al-Sabi et al. (2006)]. Studies of toxin binding provide opportunities both to probe the architecture of the sodium channel outer vestibule and also to study the selectivity of the toxins. An important step toward understanding how μCTXs target individual Na_v channel isoforms is to determine the orientation of the bound toxin within the outer vestibule of the channel.

PIIIA was the first μCTX discovered to inhibit neuronal Na_v channel isoforms (Safo et al., 2000). PIIIA is a 22-amino acid peptide with the typical disulfide framework of the μ-conotoxins (Shon et al., 1998). The similarity of PIIIA's sequence to that of μCTX GIIIA suggested that it should block skeletal muscle sodium channels, which it does, with

This work was supported by operating grants from the Canadian Institutes of Health Research [Grants MOP-10053, MOP-62690]; the Heart and Stroke Foundation of Alberta, Northwest Territory; and Nunavut. J.R.M. was supported by a studentship and G.S. was supported by a postdoctoral fellowship from Alberta Innovates Health Solutions. M.L.O. was supported by a Canadian Institutes of Health Research fellowship. R.J.F. received salary support as a Heritage Medical Scientist of the Alberta Heritage Foundation for Health Research, and D.P.T. is an Alberta Ingenuity Health Science Scientist.

Article, publication date, and citation information can be found at http://molpharm.aspetjournals.org.

doi:10.1124/mol.111.071779.

ABBREVIATIONS: Na_v, voltage-gated sodium; μCTX, μ-conotoxin; GIIIA, μ-conotoxin GIIIA; PIIIA, μ-conotoxin PIIIA; HPLC, high-performance liquid chromatography; $z\delta$, apparent valence; BTX, batrachotoxin; MD, molecular dynamics; RMSD, root-mean-square deviation; MOPS, 3-(*N*-morpholino)propanesulfonic acid.

an IC_{50} of 41 nM (IC_{50} = 19 nM for GIIIA) compared with the IC_{50} of 690 nM for neuronal Na_v channels (IC_{50}, 2.7 μM for GIIIA) (Safo et al., 2000). Energetically dominant interactions seem to occur between basic residues of the μCTXs and acidic residues of the outer charged rings within the lining of the Na_v channel extracellular vestibule (Choudhary et al., 2007). Other studies show that the Na_v channel isoform specificity is, at least partially, dictated by differences in the transmembrane segment 5–6 linker of repeat domain II (Li et al., 2001, 2003; Cummins et al., 2002). Here, a novel approach, independent of identified couplings, allows us to deduce the orientation of a bound PIIIA with respect to the Na_v channel. PIIIA's likely orientation is very similar to that of the considerably more selective but closely related toxin GIIIA.

Long, steady-state recordings from single Na_v channels incorporated into planar lipid bilayers offer a direct method to observe and analyze the kinetics and voltage dependence of potent toxins that equilibrate slowly with the channel (Krueger et al., 1983; French et al., 1984). Voltage dependence is quantified as the apparent valence, $z\delta$, of the observed block. PIIIA shows a voltage dependence of the block similar to that seen for other Na_v pore blockers including GIIIA (Becker et al., 1992), as well as tetrodotoxin, saxitoxin, and other goniotoxins (French et al., 1984; Moczydlowski et al., 1984a,b; Guo et al., 1987). This is a striking result, given the range of net charge within this heterogeneous group (Table 1). In such bilayer studies, the Na_v channels are modified by batrachotoxin to allow steady-state, single-channel analysis of binding. Analysis over a wide voltage range, for which the channel-open probability is typically >0.95, allows direct determination of kinetic parameters for toxin interactions with the open channel. This straightforward, steady-state analysis of single-channel data has clear advantages for identifying the principles underlying the voltage dependence of toxin binding and block.

Previous studies of μ-conotoxin GIIIA derivatives (Becker et al., 1992) showed a weaker voltage dependence of block for the R13Q derivative than for the native toxin, suggesting that Arg13, at least, enters the transmembrane electric field. When using the μ-conotoxin PIIIA, we substituted various amino acids to either change or to maintain charges at selected positions distributed over the surface of the toxin. We found that single charge-changing mutations, which modified the toxin's voltage dependence, $z\delta$, were localized on half the toxin. Thus, we envision a possible docking orientation in which residues that made little or no contribution to the observed voltage dependence face out of the pore, whereas those residues providing a large contribution to the voltage dependence face into the pore.

To account for these observations, two limiting mechanisms were considered, leading to the conclusion that the voltage dependence of toxin block results primarily, if not exclusively, from the redistribution of one or more Na^+ ions within the narrow part of the pore when a toxin molecule binds superficially in the pore's outer vestibule. This conclusion is consistent with the electrostatic calculations based on a simulated docking of PIIIA to a homology model of the channel.

TABLE 1
Comparison of $z\delta$ values for various Na_v channel pore blockers having different structures and nominal net charges

Toxin	PIIIA[a]	GIIIA[b]	STX, neoSTX, dcSTX[c]	TTX, B1, GTX1/2/3[d]	C1/2[e]
$z\delta$	0.59	0.58–0.73	0.60–0.68	0.58–0.69	0.59–0.72
Nominal net charge	+7	+6	+2	+1	0

STX, saxitoxin; neoSTX, *N*-1-hydroxysaxitoxin; dcSTX, decarbamoyl saxitoxin; B1, 21-sulfosaxitoxin; GTX2, 11α-hyroxysaxitoxin sulfate; GTX3, 11β-hydroxysaxitoxin sulfate; C1, 21-sulfo-11α-hyroxysaxitoxin sulfate; C2, 21-sulfo-11β-hydroxysaxitoxin sulfate; TTX, tetrodotoxin.
[a] This work.
[b] Becker et al., 1992.
[c] Krueger et al., 1983; French et al., 1984; Moczydlowski et al., 1984b; Guo et al., 1987.
[d] Moczydlowski et al., 1984a,b.
[e] Moczydlowski et al., 1984b.

Materials and Methods

Rat Skeletal Muscle Preparation. Sarcolemmal membrane vesicles were isolated from rat skeletal muscle, as described by Guo et al. (1987), using tissue obtained from one or two adult rats. The tissue was homogenized in isotonic sucrose solution by using a food processor and then centrifuged for 10 min at 5000*g*. The supernatant (S1) was filtered through six layers of cheese cloth, solid KCl was added to a concentration of 0.6 M, and the solution was stirred for 30 min. After mixing the solution to dissolve the KCl, it was centrifuged at 7974*g* for 10 min, and the supernatant (S2) was collected and centrifuged for 40 min at 160,000*g*. The pellet (P1) was resuspended in homogenization buffer (10% sucrose, 2 mg/ml sodium azide, 10 mM MOPS, pH 7.4 adjusted with NaOH or HCl), homogenized in a glass-Teflon homogenizer, and centrifuged for 10 min at 10,410*g*. The supernatant (S3) was collected and centrifuged for 40 min at 150,000*g*, and the pellet (P2) was saved. The pellet was homogenized in 10 to 20 ml of homogenization buffer and was layered on top of a sucrose gradient (35%/25% sucrose/10 mM MOPS) and centrifuged for 12 to 18 h at 90,000*g*. The band at the bottom interface was removed and centrifuged at 100,000*g* for 50 min. The resulting pellet was resuspended in a solution of 0.3 M sucrose and 20 mM HEPES to a final concentration of 1 to 3 mg/ml and stored at −80°C.

Toxin Synthesis and Preparation. Conotoxin synthesis, purification, and disulfide bond formation were performed by author D.M. and have been described in detail by Hui et al. (2002). In brief, linear peptides were synthesized by solid-phase synthesis using 9-flurenylmethoxycarbonyl chemistry. Coupling of 9-flurenylmethoxycarbonyl amino acids was performed using the 2-(1*H*-benzotriazol-1-yl)-1,1,3,3-tetramethyluronium hexafluorophosphate/1-hydroxybenzotriazole/*N*,*N*-diisopropylethylamine method on a synthesizer (431A; Applied Biosystems, Foster City, CA).

HPLC-purified linear peptide was subjected to oxidative cyclization under equilibrating conditions [i.e., air oxidation in the presence of a small amount of mercaptoethanol (10 μl in 150 ml)] to promote formation of the most stable disulfide bonds. During oxidization, the cyclization of the peptide was monitored by analytical HPLC, which was completed in 2 to 4 days at 4°C. The peptide formed a single major peak, and some minor peaks were seen in each case (the number and size of the minor peaks varied with the derivative being cyclized). The crude peptide was then isolated from the acidified reaction mixture by reverse-phase extraction, purified to near homogeneity by HPLC, and then the identity of the purified peptide was confirmed by quantitative amino acid analysis and by matrix-assisted laser desorption ionization mass spectrometric molecular weight determination.

Lyophilized conotoxin derivatives were then dissolved in purified water (~18 MΩ-cm) to a concentration of 100 mM. Toxin solutions used in the bilayer experiments were further diluted in the recording solution to the required concentration.

Single-Channel Planar Lipid Bilayer Recordings. A horizontal chamber was used for these experiments with two compartments

of ~200 μl containing the "extracellular" and "intracellular" solutions (200 mM NaCl, 10 mM HEPES, 0.1 mM EDTA, pH 7.0); for all experiments, symmetric solutions were used. The compartments were separated by a plastic partition punctured with a hole ranging from 60 to 100 μm in diameter. The current offset in symmetrical solutions was set to zero before bilayer formation. A bilayer was painted with the lipids phosphatidylethanolamine and phosphatidylcholine (phosphatidylethanolamine/phosphatidylcholine, 4:1 in decane; Avanti Polar Lipids, Alabaster, Alabama) across the hole.

An aliquot of the rat skeletal muscle membrane preparation (40 μl) was incubated with batrachotoxin (BTX; 1 μM) for a minimum of 1 h before the start of the experiments to allow BTX to bind to the channel. BTX was stored as an ethanol stock solution, and an aliquot was dried down under N_2 immediately before adding the rat membrane vesicle suspension. After incubation with BTX, the membrane preparation was then pipetted into the extracellular chamber directly over the bilayer. Channel incorporation was detected as a step increase in current of ~1 pA at ±60 mV, and channel orientation was deduced by the increased frequency of closures at −70 mV. The desired conotoxin derivative was then perfused through the extracellular chamber in two aliquots of 400 μl, and the currents were recorded at ±40 mV to allow analysis of single-channel blocking kinetics. Records on the order of hours were obtained with many distinct blocking events recorded at both voltages. All measurements were taken with an Axopatch 200 (Molecular Devices, Sunnyvale, CA) integrating patch amplifier (low-pass Bessel filter, −3 dB at 1 kHz: 80 dB/decade), filtered again with a low-pass filter at 0.1 kHz, and digitized with a Digidata 1322A 16-bit acquisition system (Molecular Devices). Experiments were recorded digitally using pCLAMP 9.2 (Molecular Devices).

Data were analyzed by determining the probability of the channel's being in the open (P_o) and toxin-bound (P_{tx}) states using Clampfit 9.2 (Molecular Devices). All steady-state records were filtered digitally after the completion of the experiment using a low-pass Gaussian filter at 20 Hz over the entire trace. A single-channel search (50% threshold) was performed to identify the open and toxin-bound intervals. Toxin-bound events were determined to be all nonconducting or reduced conductance (see *Results*) events longer than 100 ms. We calculated the dissociation constant (K_d) from the open and closed probabilities as follows:

$$K_d = \frac{[\mathrm{Tx}]P_o}{P_{tx}}$$

For each toxin derivative, K_d values were calculated at ±40 mV (n = 2–5, at each voltage for each toxin derivative). The K_d values were then plotted against voltage (millivolts) using SigmaPlot 8.0 (Systat Software, Inc., San Jose, CA). The data were fitted with linear regression using the following equation:

$$K_d(V) = K_d(0\mathrm{mV}) \exp\left(\frac{z\delta FV}{RT}\right)$$

where V is transmembrane voltage, F is the Faraday constant, R is the gas constant, and T is absolute temperature. The slope of the resulting linear regression was taken and used to calculate the effective valence for block, $z\delta$, by using the following equation:

$$z\delta = \frac{RT}{FV} \log\left(\frac{K_d(V)}{K_d(0\mathrm{mV})}\right)$$

The effective valence for block reflects the net electrical work done by all charges (toxin or nontoxin) that move within the transmembrane voltage gradient when the toxin binds. In general, if z_i is the valence of the ith charge, δ_i is the fraction of the transmembrane voltage that it traverses, and N is the total number of charges that move, then

$$z\delta = \sum_{i=1}^{N} z_i\delta_i$$

Parameter values are stated in the text as mean ± S.E.M. (n) and in all cases represent the results from two to five independent determinations ($p < 0.05$ was considered significant).

Molecular Dynamics Simulations of PIIIA Docking. The μ-conotoxin PIIIA structure was resolved using NMR experiments (Nielsen et al., 2002) and the atomic coordinates available in the Protein Data Bank (code 1R9I; (Berman et al., 2000). All molecular dynamics (MD) simulations were performed using the GROMACS set of programs (Berendsen et al., 1995; Lindahl et al., 2001). All visualization of models was performed using visual molecular dynamics (Humphrey et al., 1996). We used the AMBER99 force field for all MD simulations using the transferable intermolecular potential three-position (TIP3P) water model (Jorgensen et al., 1983). Bond lengths were constrained using the linear constraint solver (LINCS) algorithm (Hess et al., 1997). Lennard-Jones interactions were calculated with a cutoff of 0.9 nm. The electrostatic interactions were calculated using the particle mesh Ewald algorithm with real-space cutoff of 0.9 nm (Darden et al., 1993). MD simulations were performed with an integration time step of 2 fs, and the neighbor list was updated every 10 steps. The components of the system, channel, toxin, water or ions, and octane were coupled separately to a bath temperature at 310 K, using a Berendsen thermostat (Berendsen et al., 1984). After initial equilibration for 1 ns, the production runs were performed with a coupling constant of 1.5 ps. The pressure was maintained at 1 atmosphere using semi-isotropic pressure coupling to a Berendsen barostat with a coupling constant of 4 ps.

The starting channel construct (Choudhary et al., 2007) for PIIIA docking simulations was based on an extension of the model by Lipkind and Fozzard (2005). The model by Choudhary et al. (2007) incorporates a larger fraction of the sequence of the pore to which conotoxin GIIIA was docked. This channel model was embedded in the octane phase of a water-octane biphasic cell, which was used to mimic a bilayer with the GROMACS program g_membed (Wolf et al., 2010). This system contained 19,499 water molecules and 575 octane molecules, enclosed in a 83 × 88 × 110-Å box using a single sodium ion to balance the overall charge of the system. Because of the high sequence similarity and conserved disulfide bonds, a starting structure for MD simulations was obtained by superimposing PIIIA on the docked structure of GIIIA. Ten 6-ns simulations were run, with restraints on the backbone atoms of the helices using a harmonic potential of 100 $\mathrm{kJ \cdot mol^{-1} \cdot nm^{-2}}$, with 2 $\mathrm{kJ \cdot mol^{-1} \cdot nm^{-2}}$ harmonic potential restraints on the backbone atoms in the P-loops. The resulting structures were aligned to the initial conformation of the channel using a least-squares fit and clustered on the basis of the RMSD between the toxin structures using an RMSD cutoff of 0.4 nm. Clustering was performed using the algorithm implemented in the g_cluster program (Daura et al., 1999). The largest cluster that was obtained using clustering analysis contained >40% (1378) of all the structures (3001) analyzed from the 10 calculated trajectories. The central structure from this cluster was used for the electrostatic analysis described in the next section.

Electrostatic Calculations. Structural models of the toxin derivatives were created from the docked structure using the Chimera (UCSF Chimera) rotamer function. For nonalanine substitutions, the correct rotamer was chosen on the basis of the best overlap with the original residue. The native toxin and each toxin derivative in the docked conformation were used to calculate individual electrostatic potential maps using the Applied Poisson-Boltzman Solver (Baker et al., 2001) with dielectrics of 80, 10, and 2 for water, protein, and bilayer, respectively, using 200 mM salt concentration. The individual toxin derivative maps were each subtracted from the native toxin map to get an electrostatic difference-potential map, allowing us to visualize surfaces of constant "difference potential" resulting from the various charge-changing and charge-conserving substitutions in the toxin.

Results

For cellular voltage-clamp recordings, protocols of varying complexity have been applied to evaluate "use dependence" of toxin action, which reflects the combined effects of voltage dependence and state dependence of binding. Such studies are exemplified in the following citations, which also provide additional references (Salgado et al., 1986; Moran et al., 2003; Santarelli et al., 2007). Our experiments use a simpler approach, analyzing steady-state recordings from non-inactivating batrachotoxin-modified sodium channels to measure the voltage dependence of toxin binding in a voltage range for which the channels are typically open >95% of the time. Thus, although our data do not offer a critical test of state dependence, we consider the results to represent binding of toxin to the open channel.

The basic residues of PIIIA (McArthur et al., 2011), and of other μCTXs, play a vital role in toxin binding to the pore of voltage-gated sodium channels and in blocking current through the channel. Given the high sequence identity between GIIIA and PIIIA, most of the important basic residues are conserved (Fig. 1). These positively charged residues are spread over the surface of the toxin and, with the three internal disulfide bonds in the toxin, individual residues can be mutated without a large change in the overall structure of the toxin, and the binding affinity of the mutant toxin can be determined. This makes μCTXs excellent probes of voltage-gated sodium channels. We studied wild-type PIIIA plus 13 of its derivatives in which single-residue substitutions were made at seven positions distributed over the surface of the toxin. Because of the small size of the toxin and the tight backbone constraints provided by the three disulfide bonds, all of the side chains are exposed on the surface of the toxin. The various substitutions offered tests of the effects of decreasing, conserving, or increasing the charge at different points distributed over the full circumference of the toxin (Fig. 1).

Charge-Changing Amino Acid Substitutions in PIIIA Alter the Voltage Dependence of Block. The arginine at position 14 is critical to the voltage dependence of the block as well as the overall binding affinity of the toxin. On a charge-conserving mutation at this position from an arginine to a lysine, there is a decrease in the binding affinity of the toxin but little change in the overall voltage dependence of the toxin. The $z\delta$ values, presented as mean ± S.E.M. (n), were 0.59 ± 0.09 (3) for the native toxin and 0.62 ± 0.11 (4) for the R14K derivative (Fig. 2). On charge neutralization at this position, there is a significant decrease in the $z\delta$ to 0.18 ± 0.01 (3)—the same value for both the R14A and R14Q mutations. Each of these substitutions reduces the nominal net charge on the toxin from +7 to +6 at neutral pH.

Several other residues that are spread over the surface of the toxin also contribute to the overall voltage dependence of PIIIA. When the arginine or lysine at positions 12 and 17, respectively, are mutated to a charge-conserving residue (R12K or K17R), there is no significant change in the $z\delta$ values [0.64 ± 0.02 (2) for R12K and 0.60 ± 0.02 (3) for K17R] compared with native PIIIA's $z\delta$ (Fig. 3). These results suggest that charge-conserving substitutions do not change the voltage dependence. When Arg12 and Lys17 were substituted to remove a charge, the $z\delta$ values showed a significant decrease that was dependent on the location of the change. At position Arg12, when the arginine is replaced by an alanine or a glutamine, the $z\delta$ is decreased to 0.21 ± 0.01 (3) or 0.27 ± 0.01 (3), respectively. At position 17, lysine replacement by alanine or glutamine yielded a $z\delta$ value of 0.16 ± 0.01 (2) or 0.26 ± 0.01 (2), respectively. At position 20, a similar replacement of an arginine by an alanine showed a decrease in $z\delta$ to 0.32 ± 0.01 (3). This result represents a less dramatic change in $z\delta$ than for the Arg12, Arg14, and Lys17 substitutions. Replacement of the neutral Ser13 residue with a negative aspartate residue decreased $z\delta$ to 0.33 ± 0.01 (5).

Charges in Certain Positions Do Not Contribute to PIIIA Voltage Dependence. While studying different PIIIA derivatives, we found two positions at which charge neutralization or addition produced no significant change in $z\delta$. The first residue found to have no influence on $z\delta$ was the arginine at position 2 (Fig. 3). When this residue was neutralized to an alanine, the $z\delta$ was 0.45 ± 0.03 (2). This value of $z\delta$ was not significantly different from that for the native toxin. Simulated docking of GIIIA indicated that the analogous residue, Arg1, is located on the outer surface of the docked toxin with respect to the channel (Choudhary et al., 2007). The other position observed to have no significant influence on $z\delta$ was the glycine at position 6. In this case, we substituted a positively charged lysine at this position, which yielded a $z\delta$ of 0.54 ± 0.02 (3), again not significantly differ-

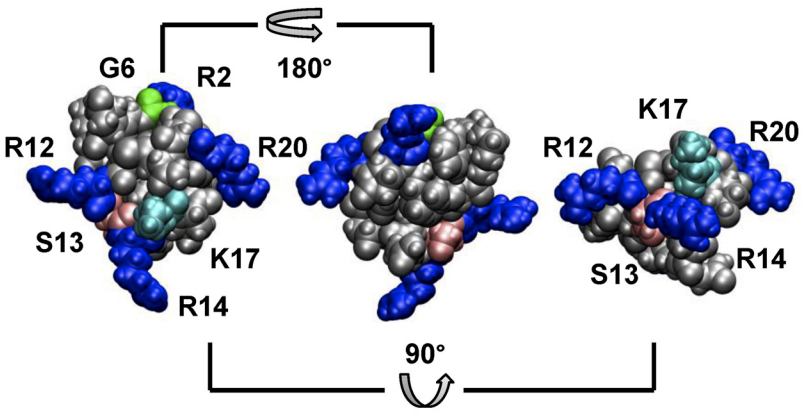

Conotoxin	1	2	3	4	5	6	7	8	9	10	11	12	13	14	15	16	17	18	19	20	21	22	23
GIIIA		R	D	C	C	T	O	O	K	K	C	K	D	R	Q	C	K	O	Q	R	C	C	A#
PIIIA	Z	R	L	C	C	G	F	O	K	S	C	R	S	R	Q	C	K	O	H	R	C	C#	

Fig. 1. Solution structure of PIIIA. Top, the important amino acids shown from three different viewpoints with basic residues in blue (arginine, dark blue; lysine, cyan), serine in pink, and glycine in green. Bottom, sequence alignment of PIIIA and GIIIA (numbering based on PIIIA).

ent from the value for the native toxin. The analogous residue in GIIIA, the threonine at position 5, was also located on the exposed outer surface of the docked toxin, close to the arginine at position 1.

Simulations of PIIIA Docking into a Sodium Channel Model. PIIIA simulations were first run in a water bath to determine the structural stability of the toxin. The molecular dynamics simulations were run for 20 ns, allowing the toxin

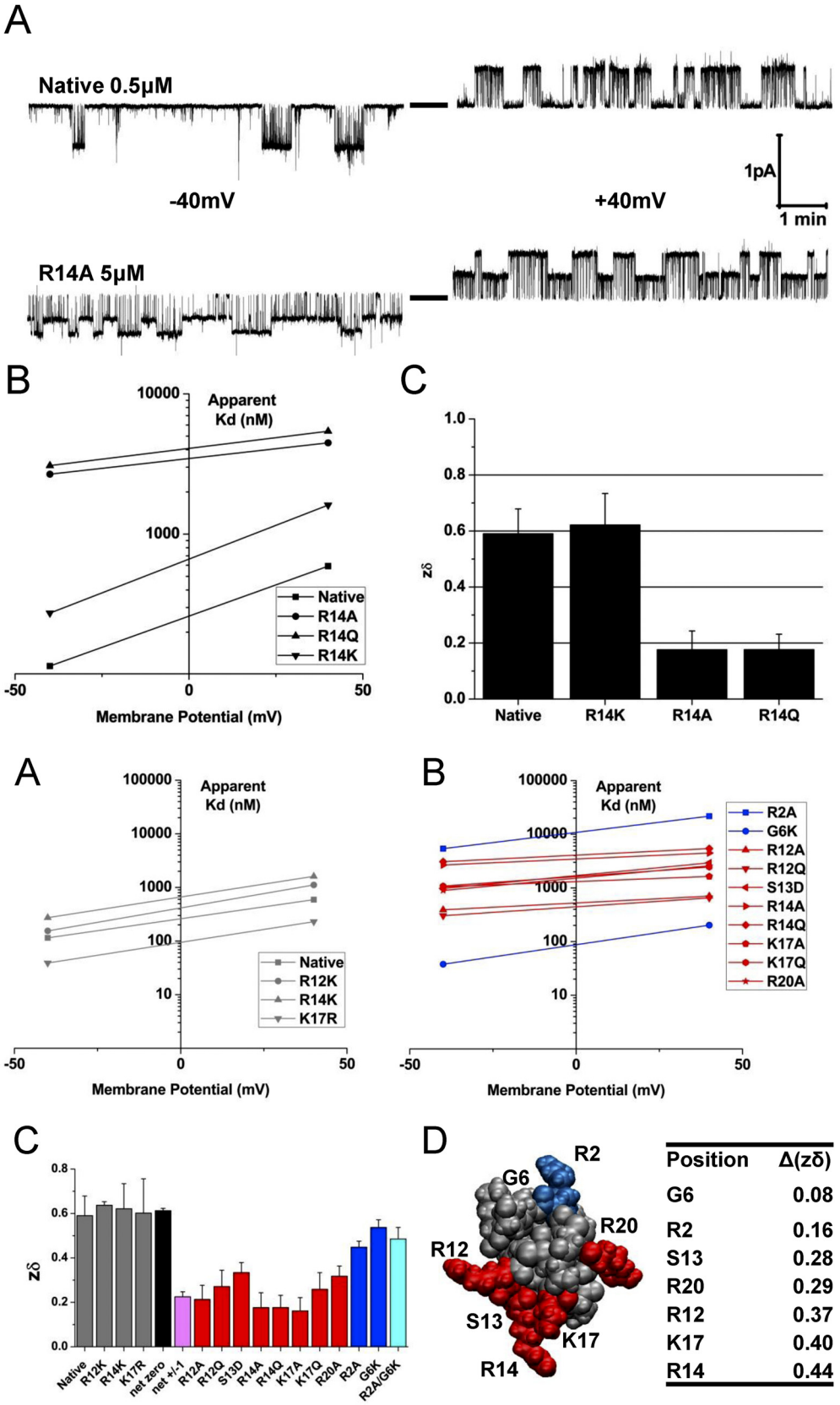

Position	Δ(zδ)
G6	0.08
R2	0.16
S13	0.28
R20	0.29
R12	0.37
K17	0.40
R14	0.44

Fig. 2. Charge neutralization at position 14 induces a clear change in the voltage dependence of block. A, current traces from single sodium channel in the presence of native PIIIA and R14A showing the typical voltage dependence of toxin block. Note that R14A only blocks a fraction of the unitary current on binding. Left traces, −40 mV; right, +40 mV. B, voltage dependencies of apparent K_d for PIIIA derivatives with different substitutions at position Arg14, showing both charge-changing and charge-neutralization mutations. C, $z\delta$ values calculated from the slopes in part B for substitutions in the Arg14 position.

Fig. 3. Charge-changing mutations over the surface of PIIIA show varying degrees of changes in voltage dependence, which map systematically on to the surface of the toxin. A, voltage dependence of PIIIA showing all charge-conserving mutations. B, voltage dependence of PIIIA showing all charge-changing mutations. C, $z\delta$ values calculated from the slopes in A and B for both charge-conserving and addition/neutralization groups (net zero denotes the mean for all charge-conserving derivatives; net ±1 denotes the mean for charge additions/neutralizations except R2A and G6K; R2A/G6K denotes the mean for R2A and G6K). D, structure of PIIIA showing residues important in the overall voltage dependence (red) and those not important in voltage dependence (blue). Mean values of changes in $z\delta$, for substitutions at each position, are tabulated alongside, as $\Delta(z\delta)$.

to move freely with no restraints placed on the toxin residues. The final toxin structures showed little change over the course of the simulation (backbone RMSD ≈ 2 Å), with the main structural differences in the N terminus.

The toxin structure was then aligned with the GIIIA-docked structure in the sodium channel pore model (Choudhary et al., 2007). Ten 6-ns MD simulations were run and the results were clustered, with the center structure of the largest cluster shown in Fig. 4, along with the starting structure. The center structure of the cluster moved slightly lower into the pore from the starting structure and rotated slightly, moving the critical arginine closer to the domain II and III inner-ring residues.

Toxin Charge Distribution Systematically Biases the Electrostatic Potential in the Pore. The central structure of the largest cluster from the MD simulations was used to calculate electrostatic difference-potential maps and were visualized using Chimera (Fig. 5). Electrostatic difference-potential maps, with respect to the docked native PIIIA, were calculated for derivatives G6K, R12A/Q, S13D, R14A/Q, K17A/Q, and R20A. Each derivative's electrostatic potential map was subtracted from the native PIIIA map to yield the individual electrostatic difference-potential map. Difference-potential surfaces are expected to be a more robust estimate of the electrostatic effects of discrete amino acid substitutions in the toxin than the estimates of overall electrostatic potential, given the lack of a high-resolution structure for the channel. Figure 5 shows the difference-potential surfaces for R2A, R12A, and R14A with a solid cyan surface (2 kT/e), or a red mesh (1 kT/e), representing changes in the electrostatic potential at different distances from the site of the charge change. Notice that the volume enclosed by these surfaces is obviously largest for R14A, the position deepest in the pore, and smallest for R2A, which is directly exposed to the screening effects of the salt (200 mM) in the experimental bathing solution.

Discussion

Many external inhibitors of voltage-gated sodium channels act by directly blocking current through the pore. These pore blockers bind to site 1 (Catterall et al., 2005) on the sodium channel, thus preventing the flow of sodium through the channel. In steady-state recordings, block is dependent on the applied voltage. Classic pore blockers such as tetrodo-

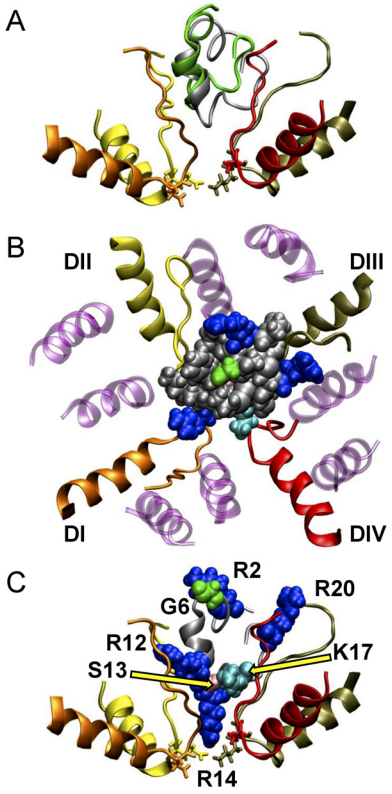

Fig. 4. MD simulation of docking of PIIIA into the vestibule of a voltage-gated sodium channel. Depths of different residues in the channel vestibule are consistent with the observed voltage dependencies for block by different derivatives. A, initial and final structures for the molecular dynamics docking simulations showing toxin backbone in green (start) and gray (final). Domains: I, orange; II, yellow; III, tan; and IV, red. B, top view of center structure of largest cluster. C, side view of center structure of largest cluster, with all residues used in $z\delta$ calculations shown.

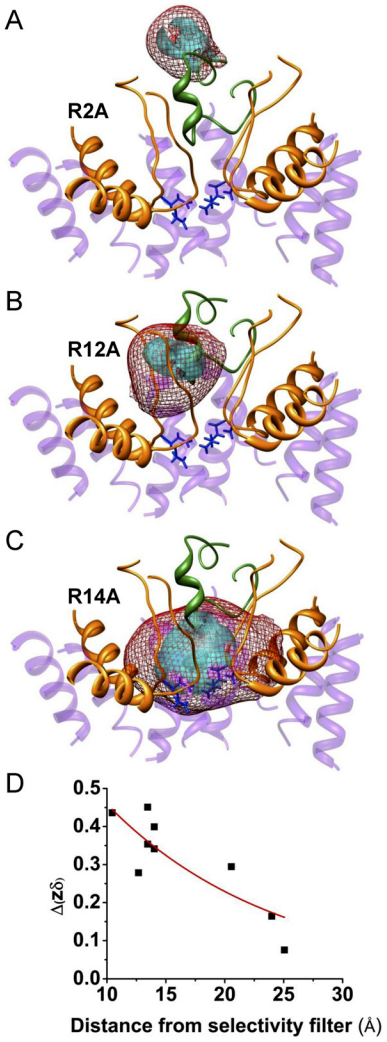

Fig. 5. Electrostatic difference-potential maps for substitutions at different positions. Only toxin charges that closely approach the DEKA selectivity ring (colored side chains in stick format) would significantly influence Na^+ distribution in the pore. A, R2A; B, R12A; and C, R14A. Difference-potential surfaces are depicted for 2kT/e (cyan) and for 1kT/e (red mesh) and represent the changes in electrostatic potential with unit charge changes at the specified location. D, graph of experimental $\Delta(z\delta)$ values versus model distance from a point centered between the four selectivity filter Cα residues to the appropriate Cα residue of the toxin.

toxin and saxitoxin show $z\delta$ values similar to those for the μCTXs, regardless of the overall charge on the toxin (Krueger et al., 1983; French et al., 1984; Moczydlowski et al., 1984a,b). Moczydlowski et al. (1984a,b) arrived at a "hypothesis of last resort" that the observed voltage dependence of toxin block resulted from a voltage-dependent conformational change within the Na_v channel protein when the toxin binds. Although we agree with Moczydlowski et al. (1984a,b) that toxin charges are unlikely to enter deeply into the voltage gradient, our own data raise the intriguing alternate possibility that toxin charges could produce the voltage dependence by electrostatically inducing sodium ions to traverse a substantial part of the transmembrane voltage (Fig. 6).

μCTXs have numerous basic residues that could contribute to the overall voltage dependence of binding and block. To examine the contributions of individual amino acids, we made PIIIA derivatives with charge-conserving or charge-changing amino acid substitutions. Various charge-conserving substitutions over the surface of PIIIA yielded derivatives showing voltage dependence similar to that of the native toxin ($z\delta\delta \sim 0.6$). Replacement of certain positive residues by neutral ones led to decreases in $z\delta$, which initially seemed to suggest that these residues traverse part of the transmembrane electric field when the toxin binds. Changes in $z\delta$ associated with different substitutions suggested an orientation of the bound toxin in harmony with analyses of partial single-channel block and interacting residue pairs on toxin and channel (Hui et al., 2002; Choudhary et al., 2007).

Charge-changing mutations at positions 12, 13, 14, 17, and 20 affected the voltage dependence to varying degrees [$\Delta(z\delta) = 0.25–0.43$], whereas mutations of Arg2 and Gly6 had no effect. The data suggest a toxin orientation with residues at positions 12, 14, 17, and 20 placed deep in the vestibule, whereas those at positions 2 and 6 faced out into the extracellular solution. In the simulated docking of the closely related μCTX, GIIIA (Choudhary et al., 2007), we see the homologous four residues (Lys11, Arg13, Lys16, and Arg19) lying inside the pore, whereas Arg1 and Thr5, which align with Arg2 and Gly6 of PIIIA, face the extracellular solutions. These two sets of results are based on distinct techniques and principles. Our present analysis attempts to locate toxin residues with respect to the electrical potential profile across the channel, whereas the GIIIA docking was constrained by toxin-channel coupling energies calculated from mutant cycle analysis. These fundamentally different approaches converge to imply very similar orientations of the bound toxin. Figure 4B shows PIIIA binding in an orientation similar to that predicted for GIIIA. This reveals a systematic consistency of the GIIIA coupling energy constraints with our $z\delta$ results (Figs. 3D and 4).

Looking more quantitatively, the sum of the mean $\Delta(z\delta)$ values for neutralization of PIIIA's five basic residues (Fig. 3D) is 1.66, compared with 0.59, the $z\delta$ value for the wild-type toxin. In addition, native site 1 "pore blockers" (Table 1) all show $z\delta$ values of 0.59 to 0.74 independent of the net charge on the toxin (GIIIA +6, PIIIA +7, tetrodotoxin +1, saxitoxin and its derivatives, +2 to 0) (Cruz et al., 1985; Guo et al., 1987). Thus, we cannot account for voltage dependence of the wild type as the sum of contributions from individual charges, despite evidence that toxin-bound orientation is maintained after single-residue substitutions.

This enigmatic result might be explained if a part, or perhaps even all, of the $z\delta$ reflected movement of a nontoxin charge, such as a sodium ion, within the transmembrane electric field in synchrony with toxin binding. Previously, we obtained two clear lines of evidence for electrostatic interactions between bound μCTX derivatives and Na^+ ions in the conducting pathway. First, when peptides of the form GIIIA-R13X dock, they allow a residual single-channel current through the toxin-bound channel, and the magnitude of the residual current depends systematically on the charge and size of the substituent residue (Hui et al., 2002). Second, single-channel conductance-concentration relations show that the sodium binding in the pore is weakened by pre-docked toxin (Pavlov et al., 2008). Thus, if the toxin binds close to, but outside, the region of steep potential change, a single sodium ion may be forced by electrostatic repulsion to move within the membrane electric field. This would result in similar $z\delta$ values that would not be well correlated with the total charge on the toxin but depend on one, or a subset, of the neighboring toxin charges. The measured $z\delta$ would then primarily reflect the movement of a sodium ion, not the toxin charge, traversing part of the applied electric field. Nonetheless, this does not alter the deduced toxin orientation because an individual residue (e.g., Arg14), which extends relatively deeply into the pore vestibule, would have a stronger interaction with a sodium ion in the pore than a residue at a more superficial position (Fig. 5).

This explanation fits with previous studies examining charybdotoxin block of Shaker potassium channels in which the voltage dependence required the presence a particular toxin charge (Lys27), as well as permeant or blocking alkali cations that could access the inner vestibule of the channel (Goldstein and Miller, 1993). Overall, those authors concluded that most of the voltage dependence resulted from a toxin-alkali cation interaction, with a minor contribution from the key pore-blocking Lys27 residue on the toxin.

Two plausible limiting hypotheses to explain our observed $\Delta(z\delta)$ values are illustrated in Fig. 6. Either model could account for the toxin charge-dependent changes in voltage

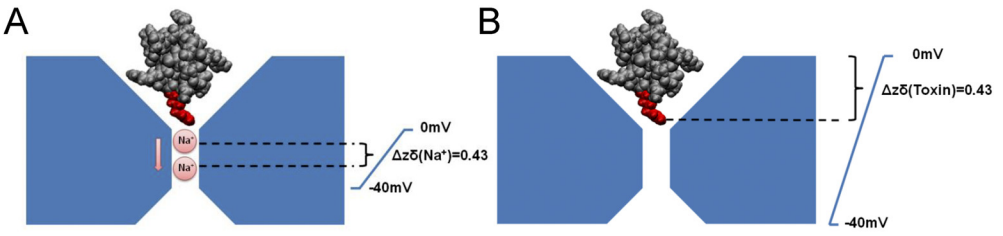

Fig. 6. Diagrams of possible mechanisms for the observed voltage dependence of block. Indicated $\Delta(z\delta)$ values are those for a unit charge change at Arg14. A, toxin charge does not enter the applied voltage gradient. The voltage dependence results entirely from displacement of a permeant ion (Na^+) within the electric field. B, a toxin charge (Arg14) penetrates part of the transmembrane potential difference, and its replacement contributes directly to the observed change in $z\delta$. In this extreme scenario, there is no redistribution of Na^+ within the channel on toxin binding.

dependence, but only Fig. 6A takes into account interactions between permeant ions and the bound toxin and is consistent with our present data. To further scrutinize this possibility, we used the Applied Poisson-Boltzman Solver (see *Materials and Methods*) to estimate changes in the electrostatic potential in and near the pore vestibule when various toxin derivatives are bound. Residues that are positioned most deeply in the vestibule, when the toxin is bound, induce the largest changes in electrostatic potential near the DEKA selectivity motif (Fig. 5C), where a single sodium ion might be expected to bind in the absence of toxin. These calculations show that Arg14 and Lys17 have the largest effects (~1–2 kT/e) and predict that residues such as Arg12, S13D, and Arg20 exert a weaker influence. Residues Arg2 and Gly6 (Fig. 5A) showed no significant effect on the electrostatic potential in the pore, consistent with their lack of effect on the voltage dependence of PIIIA binding.

It remains possible that the actual mechanism involves an intermediate case, between the two presented in Fig. 5, in which the changes in $z\delta$ include a small component contributed by side-chain charges entering the transmembrane electric field, with most of the toxin voltage dependence associated with the movement of a permeant ion(s) in the pore. This is similar to the conclusions from studies of charybdotoxin block of Shaker channels (Goldstein and Miller, 1993), with one striking quantitative difference: for charybdotoxin block of Shaker channels, voltage dependence relies exclusively on one toxin residue, Lys27, the side chain of which seems to enter the extended, narrow K channel selectivity filter.

Overall, three results combine to support the conclusion that the observed voltage dependence of μCTX block results from the movement of a sodium ion from a preferred binding site within the transmembrane electric field when the toxin binds to the channel. First, the sum of observed changes in $z\delta$ for substitutions at individual positions in PIIIA is greater than the $z\delta$ for wild-type toxin binding. Second, various site 1 toxins with different net charges show similar voltage dependencies. Third, there is a change in sodium affinity for its preferred binding site when a partially blocking μCTX (GIIIA-R14Q) is bound (Pavlov et al., 2008). Unlike potassium channels, in which potassium ions are tightly coupled and pass through the channel in single file (Hodgkin and Keynes, 1955), sodium channels show only relatively weak ion-ion coupling (Begenisich and Busath, 1981; French et al., 1994), which suggests that, most of the time, only a single sodium ion is bound within the pore. We argue that displacement of sodium from this binding site underlies most of the observed voltage dependence of these pore blockers. Despite the sequence homology and apparent similarity in binding orientations of GIIIA and PIIIA, PIIIA shows interactions with both muscle and neuronal Na_v channels (Shon et al., 1998), whereas GIIIA is highly specific for adult skeletal muscle channels (Cruz et al., 1989). Thus, these two toxins, along with their smaller, neuron-selective homolog μCTX KIIIA (Bulaj et al., 2005; Zhang et al., 2007), achieve very different specificity, while maintaining a generally similar orientation when bound to the channel.

Acknowledgments

We thank Dr. Gerald Zamponi for comments on a draft of the manuscript.

Authorship Contributions

Participated in research Design: McArthur, Singh, Tieleman, and French.

Conducted experiments: McArthur, Singh, and Ostroumov.

Contributed new reagents or analytic tools: McArthur, O'Mara, McMaster, Tieleman, and French.

Performed data analysis: McArthur, Singh, and French.

Wrote or contributed to the writing of the manuscript: McArthur, Singh, Tieleman, and French.

References

Al-Sabi A, McArthur J, Ostroumov V, and French RJ (2006) Marine toxins that target voltage-gated sodium channels. *Marine Drugs* **4:**157–192.

Baker NA, Sept D, Joseph S, Holst MJ, and McCammon JA (2001) Electrostatics of nanosystems: application to microtubules and the ribosome. *Proc Natl Acad Sci USA* **98:**10037–10041.

Becker S, Prusak-Sochaczewski E, Zamponi G, Beck-Sickinger AG, Gordon RD, and French RJ (1992) Action of derivatives of mu-conotoxin GIIIA on sodium channels. Single amino acid substitutions in the toxin separately affect association and dissociation rates. *Biochemistry* **31:**8229–8238.

Begenisich T and Busath D (1981) Sodium flux ratio in voltage-clamped squid giant axons. *J Gen Physiol* **77:**489–502.

Berendsen HJC, Postma JPM, Vangunsteren WF, Dinola A, and Haak JR (1984) Molecular dynamics with coupling to an external bath. *J Chem Phys* **81:**3684–3690.

Berendsen HJC, van der Spoel D, and van Drunen R (1995) GROMACS: a message-passing parallel molecular dynamics implementation. *Comp Phys Commun* **91:**43–56.

Berman HM, Westbrook J, Feng Z, Gilliland G, Bhat TN, Weissig H, Shindyalov IN, and Bourne PE (2000) The Protein Data Bank. *Nucleic Acids Res* **28:**235–242.

Bulaj G, West PJ, Garrett JE, Watkins M, Marsh M, Zhang MM, Norton RS, Smith BJ, Yoshikami D, and Olivera BM (2005) Novel conotoxins from Conus striatus and Conus kinoshitai selectively block TTX-resistant sodium channels. *Biochemistry* **44:**7259–7265.

Catterall WA, Goldin AL, and Waxman SG (2005) International Union of Pharmacology. XLVII. Nomenclature and structure-function relationships of voltage-gated sodium channels. *Pharmacol Rev* **57:**397–409.

Choudhary G, Aliste MP, Tieleman DP, French RJ, and Dudley SC Jr (2007) Docking of mu-conotoxin GIIIA in the sodium channel outer vestibule. *Channels* **1:**344–352.

Cruz LJ, Gray WR, Olivera BM, Zeikus RD, Kerr L, Yoshikami D, and Moczydlowski E (1985) *Conus geographus* toxins that discriminate between neuronal and muscle sodium channels. *J Biol Chem* **260:**9280–9288.

Cruz LJ, Kupryszewski G, LeCheminant GW, Gray WR, Olivera BM, and Rivier J (1989) mu-Conotoxin GIIIA, a peptide ligand for muscle sodium channels: chemical synthesis, radiolabeling, and receptor characterization. *Biochemistry* **28:**3437–3442.

Cummins TR, Aglieco F, and Dib-Hajj SD (2002) Critical molecular determinants of voltage-gated sodium channel sensitivity to mu-conotoxins GIIIA/B. *Mol Pharmacol* **61:**1192–1201.

Darden T, York D, and Pedersen L (1993) Particle mesh Ewald: an N · Log(N) method for Ewald sums in large systems. *J Chem Phys* **98:**10089–10092.

Daura X, Gademann K, Jaun B, Seebach D, van Gunsteren WF, and Mark AE (1999) Peptide folding: when simulation meets experiment. *Angew Chem Int Ed Engl* **38:**236–240.

French RJ, Worley JF 3rd, and Krueger BK (1984) Voltage-dependent block by saxitoxin of sodium channels incorporated into planar lipid bilayers. *Biophys J* **45:**301–310.

French RJ, Worley JF 3rd, Wonderlin WF, Kularatna AS, and Krueger BK (1994) Ion permeation, divalent ion block, and chemical modifications of single sodium channels. Description by single- and double-occupancy rate-theory models. *J Gen Physiol* **103:**447–470.

Goldstein SA and Miller C (1993) Mechanism of charybdotoxin block of a voltage-gated K^+ channel. *Biophys J* **65:**1613–1619.

Guo XT, Uehara A, Ravindran A, Bryant SH, Hall S, and Moczydlowski E (1987) Kinetic basis for insensitivity to tetrodotoxin and saxitoxin in sodium channels of canine heart and denervated rat skeletal muscle. *Biochemistry* **26:**7546–7556.

Hess B, Bekker H, Berendsen HJC, and Fraaije JGEM (1997) LINCS: a linear constraint solver for molecular simulations. *J Comput Chem* **18:**1463–1472.

Hodgkin AL and Keynes RD (1955) The potassium permeability of a giant nerve fibre. *J Physiol* **128:**61–88.

Hui K, Lipkind G, Fozzard HA, and French RJ (2002) Electrostatic and steric contributions to block of the skeletal muscle sodium channel by mu-conotoxin. *J Gen Physiol* **119:**45–54.

Humphrey W, Dalke A, and Schulten K (1996) VMD: visual molecular dynamics. *J Mol Graph* **14:**33–38, 27–28.

Jorgensen WL, Chandrasekhar J, Madura JD, Impey RW, and Klein ML (1983) Comparison of simple potential functions for simulating liquid water. *J Chem Phys* **79:**926–935.

Krueger BK, Worley JF 3rd, and French RJ (1983) Single sodium channels from rat brain incorporated into planar lipid bilayer membranes. *Nature* **303:**172–175.

Li RA, Ennis IL, Tomaselli GF, French RJ, and Marbán E (2001) Latent specificity of molecular recognition in sodium channels engineered to discriminate between two "indistinguishable" mu-conotoxins. *Biochemistry* **40:**6002–6008.

Li RA, Ennis IL, Xue T, Nguyen HM, Tomaselli GF, Goldin AL, and Marbán E (2003) Molecular basis of isoform-specific micro-conotoxin block of cardiac, skeletal muscle, and brain Na^+ channels. *J Biol Chem* **278:**8717–8724.

Lindahl E, Hess B, and van der Spoel D (2001) GROMACS 3.0: a package for molecular simulation and trajectory analysis. *J Mol Model* **7:**306–317.

Lipkind GM and Fozzard HA (2005) Molecular modeling of local anesthetic drug binding by voltage-gated sodium channels. *Mol Pharmacol* **68:**1611–1622.
McArthur JR, Ostroumov V, Al Sabi, McMaster D, and French RJ (2011) Multiple, distributed interactions of mu-conotoxin PIIIA associated with broad targeting among voltage-gated sodium channels. *Biochemistry* **50:**116–124.
Moczydlowski E, Garber SS, and Miller C (1984a) Batrachotoxin-activated Na_+ channels in planar lipid bilayers. Competition of tetrodotoxin block by Na^+. *J Gen Physiol* **84:**665–686.
Moczydlowski E, Hall S, Garber SS, Strichartz GS, and Miller C (1984b) Voltage-dependent blockade of muscle Na^+ channels by guanidinium toxins. *J Gen Physiol* **84:**687–704.
Moran O, Picollo A, and Conti F (2003) Tonic and phasic guanidinium toxin-block of skeletal muscle Na channels expressed in mammalian cells. *Biophys J* **84:**2999–3006.
Nielsen KJ, Watson M, Adams DJ, Hammarström AK, Gage PW, Hill JM, Craik DJ, Thomas L, Adams D, Alewood PF, et al. (2002) Solution structure of mu-conotoxin PIIIA, a preferential inhibitor of persistent tetrodotoxin-sensitive sodium channels. *J Biol Chem* **277:**27247–27255.
Pavlov E, Britvina T, McArthur JR, Ma Q, Sierralta I, Zamponi GW, and French RJ (2008) Trans-channel interactions in batrachotoxin-modified skeletal muscle sodium channels: voltage-dependent block by cytoplasmic amines, and the influence of mu-conotoxin GIIIA derivatives and permeant ions. *Biophys J* **95:**4277–4288.
Safo P, Rosenbaum T, Shcherbatko A, Choi DY, Han E, Toledo-Aral JJ, Olivera BM, Brehm P, and Mandel G (2000) Distinction among neuronal subtypes of voltage-activated sodium channels by mu-conotoxin PIIIA. *J Neurosci* **20:**76–80.
Salgado VL, Yeh JZ, and Narahashi T (1986) Use- and voltage-dependent block of the sodium channel by saxitoxin. *Ann NY Acad Sci* **479:**84–95.
Santarelli VP, Eastwood AL, Dougherty DA, Horn R, and Ahern CA (2007) A cation-pi interaction discriminates among sodium channels that are either sensitive or resistant to tetrodotoxin block. *J Biol Chem* **282:**8044–8051.
Shon KJ, Olivera BM, Watkins M, Jacobsen RB, Gray WR, Floresca CZ, Cruz LJ, Hillyard DR, Brink A, Terlau H, et al. (1998) mu-Conotoxin PIIIA, a new peptide for discriminating among tetrodotoxin-sensitive Na channel subtypes. *J Neurosci* **18:**4473–4481.
Wolf MG, Hoefling M, Aponte-Santamaría C, Grubmüller H, and Groenhof G (2010) g_membed: efficient insertion of a membrane protein into an equilibrated lipid bilayer with minimal perturbation. *J Comput Chem* **31:**2169–2174.
Zhang MM, Green BR, Catlin P, Fiedler B, Azam L, Chadwick A, Terlau H, McArthur JR, French RJ, Gulyas J, et al. (2007) Structure/function characterization of micro-conotoxin KIIIA, an analgesic, nearly irreversible blocker of mammalian neuronal sodium channels. *J Biol Chem* **282:**30699–30706.

Address correspondence to: Dr. Robert J. French, Physiology and Biophysics, University of Calgary, 3330 Hospital Dr. NW, Calgary, AB T2N 4N1. E-mail: french@ucalgary.ca